Journal of Inorganic Biochemistry 104 (2010) 893–901

Contents lists available at ScienceDirect

Journal of Inorganic Biochemistry

journal homepage: www.elsevier.com/locate/jinorgbio

A theoretical study of Ru(II) polypyridyl DNA intercalators Structure and electronic absorption spectroscopy of $[Ru(phen)_2(dppz)]^{2+}$ and $[Ru(tap)_2(dppz)]^{2+}$ complexes intercalated in guanine–cytosine base pairs

David Ambrosek [a,1], Pierre-François Loos [b,2], Xavier Assfeld [b], Chantal Daniel [a,*]

[a] Laboratoire de Chimie Quantique, Institut de Chimie UMR 7177 CNRS/Université de Strasbourg 4 rue Blaise Pascal 67000 Strasbourg, France
[b] Laboratoire de Chimie et Biochimie Théorique UMR 7565 CNRS/Université Henri Poincaré 54 506 Vandoeuvre Les Nancy, France

ARTICLE INFO

Article history:
Received 29 June 2009
Received in revised form 1 April 2010
Accepted 2 April 2010
Available online 14 April 2010

Keywords:
Ruthenium complexes
Intercalation
Structure
Absorption spectroscopy
Density functional theory

ABSTRACT

The structural and spectroscopic properties of $[Ru(phen)_2(dppz)]^{2+}$ and $[Ru(tap)_2(dppz)]^{2+}$ (phen = 1,10-phenanthroline; tap = 1,4,5,8-tetraazaphenanthrene; dppz = dipyridophenazine) have been investigated by means of density functional theory (DFT), time-dependent DFT (TD–DFT) within the polarized continuum model (IEF–PCM) and quantum mechanics/molecular mechanics (QM/MM) calculations. The model of the Δ and Λ enantiomers of Ru(II) intercalated in DNA in the minor and major grooves is limited to the metal complexes intercalated in two guanine–cytosine base pairs. The main experimental spectral features of these complexes reported in DNA or synthetic polynucleotides are better reproduced by the theoretical absorption spectra of the Δ enantiomers regardless of intercalation mode (major or minor groove). This is especially true for $[Ru(phen)_2(dppz)]^{2+}$. The visible absorption of $[Ru(tap)_2(dppz)]^{2+}$ is governed by the $MLCT_{tap}$ transitions regardless of the environment (water, acetonitrile or bases pair), the visible absorption of $[Ru(phen)_2(dppz)]^{2+}$ is characterized by transitions to metal-to-ligand-charge-transfer $MLCT_{dppz}$ in water and acetonitrile and to $MLCT_{phen}$ when intercalated in DNA. The response of the IL_{dppz} state to the environment is very sensitive. In vacuum, water and acetonitrile these transitions are characterized by significant oscillator strengths and their positions depend significantly on the medium with blue shifts of about 80 nm when going from vacuum to solvent. When the complex is intercalated in the guanine–cytosine base pairs the $^1IL_{dppz}$ transition contributes mainly to the band at 370 nm observed in the spectrum of $[Ru(phen)_2(dppz)]^{2+}$ and to the band at 362 nm observed in the spectrum of $[Ru(tap)_2(dppz)]^{2+}$.

1. Introduction

Since the discovery of ruthenium complexes as potentially highly sensitive luminescent reporters of DNA in aqueous environments and as therapeutic and diagnostic agents by the team of J. K. Barton in the late 80s [1] considerable interest has been given to the spectroscopic properties of this class of molecules. Absorption and emission spectral features of a series of $[Ru(L)_2(L')]^{2+}$ complexes (L = bipyridine, 1,10 phenanthroline (phen) and 1,4,5,8 tetraazaphenanthrene (tap) and L' = dipyridophenazine (dppz) and related derivatives) have been investigated by UV/visible and circular dichroism in various environments such as water, acetonitrile, synthetic polynucleotides and calf thymus DNA [2–19]. The literature devoted to the spectroscopic properties of $[Ru(phen)_2(dppz)]^{2+}$ and $[Ru(tap)_2(dppz)]^{2+}$ is particularly abundant with absorption/emission data reported in H_2O, CH_3CN, for the Ru(II) complexes bound to the double-stranded synthetic polynucleotides $[poly(dG–dC)]_2$ (G = guanine, and C = cytosine) [2–4,6,7,10,11,13,14] and in the presence of calf thymus DNA (CT–DNA).

The electronic absorption spectrum of $[Ru(phen)_2(dppz)]^{2+}$ is characterized by an absorption at 440 nm observed in H_2O, CH_3CN as well as in synthetic polynucleotides or CT–DNA [6,7,11,13]. The corresponding absorption is red shifted to around 460 nm in $[Ru(tap)_2(dppz)]^{2+}$ (452 nm in H_2O, 454 nm in CH_3CN and 462 nm in CT–DNA) [13]. The tap substituted complex possesses an extra band at 412 nm. The spectral region between 460 nm and 400 nm is not sensitive to the environment and has been attributed to metal-to-ligand-charge-transfer (MLCT) states, most probably to the ancillary ligands although experimentally it is extremely difficult to distinguish between MLCT states localized on the ancillary ligands or on the dppz ligand. Both complexes are characterized by a band around 360 nm, assigned to an Intra-Ligand (IL) state localized on the dppz ligand that is strongly affected by the environment and distinguished by an important hypochromic effect upon CT–DNA addition or by interaction with polynucleotides. This decrease in intensity (compared to absorption in the absence of CT–DNA) has been attributed to the intercalation and consequently the stacking of the dppz ligand with the base pairs. Below

* Corresponding author. Fax: +33 3 68851314.
E-mail address: c.daniel@chimie.u-strasbg.fr (C. Daniel).
[1] Present address: Institute of Physics, Rostock University, 18051 Rostock, Germany.
[2] Present address: Research School of Chemistry, Australian National University, Canberra ACT 0200, Australia.

0162-0134/$ – see front matter © 2010 Elsevier Inc. All rights reserved.
doi:10.1016/j.jinorgbio.2010.04.002

320 nm, the DNA absorption region, the absorption spectra of the intercalated complexes are difficult to interpret but are characterized by a strong absorption with maxima around 290 nm, as compared to the peaks observed at 264 nm and 278 nm respectively for the phen and tap complexes in either H_2O or CH_3CN. Whereas the absorption spectra of $[Ru(phen)_2(dppz)]^{2+}$ and $[Ru(tap)_2(dppz)]^{2+}$ do not differ dramatically and are not significantly affected by the environment their emissive properties are influenced by the experimental conditions.

The emission yield of the phen substituted complex is undetectable in water, moderate in acetonitrile (630 nm) and intensifies when the complex is intercalated in CT–DNA or bound to polynucleotides [7]. Pure enantiomers Δ and Λ of $[Ru(phen)_2(dppz)]^{2+}$ have been studied and it has been shown that the Δ enantiomer is primarily responsible for the luminescence enhancement upon DNA binding [4]. The efficient quenching of luminescence in water has been proposed to be due to fast hydrogen bonding of solvent to the phenazine aza nitrogens of the dppz radical anion formed in some MLCT states [20]. Whereas $[Ru(tap)_2(dppz)]^{2+}$ is characterized by detectable emissive properties both in water (636 nm, $\phi_{em} = 0.035$, $\tau = 820$ ns) and in acetonitrile (621 nm), the emission is quenched when the complex is intercalated in CT–DNA or bound to $[poly(dG–dC)]_2$ [10]. This quenching is consistent with an electron transfer process from the guanine to the excited complex and evidenced by the formation of $[Ru(tap)_2(dppz)]^{+}$ within 480 ± 40 ps [13]. Despite the large number of experimental studies reported on these complexes over the past 10 years, few theoretical studies have been performed. These studies have often focused either on structural or binding mode aspects [21,22] or on the nature and position of the low-lying triplet excited states. The spectroscopic calculations, based essentially on semi-empirical [22,23] or time-dependent density functional theory TD–DFT [24–26] approaches show that the low-lying MLCT states delocalized over the three ligands in the free complex are slightly red shifted and re-localize on the ancillary and dppz ligands upon binding to DNA. On the basis of TD–DFT results the experimental band at 440 nm in the spectrum of $[Ru(phen)_2(dppz)]^{2+}$ has been attributed to a superposition of $MLCT_{dppz}$ and $MLCT_{phen}$ transitions calculated at about 450 nm and 415 nm, respectively. The band near 360 nm has been assigned to a state with dominant MLCT character mixed with an IL_{dppz} [24]. TD–DFT calculations based on Car–Parrinello optimized singlet and triplet geometries of $[Ru(phen)_2(dppz)]^{2+}$ intercalated into an adenine-thymine tetramer $d(ATAT)_2$ point to the presence of low-lying singlet states mainly originating from adenine or thymine-localized orbitals and calculated at 510 nm, 482 nm and 479 nm [25].

In order to decipher the complicated photophysics which underlie the observed absorption/emission properties of $[Ru(phen)_2(dppz)]^{2+}$ and $[Ru(tap)_2(dppz)]^{2+}$ and to investigate the mechanism of the molecular light switch effect in this class of molecules we have studied the structures and the absorption spectroscopy of both complexes on the basis of DFT and TD–DFT methods. The calculations have been performed either in vacuum or with solvent corrections by means of the polarized continuum model (PCM) for a few states [27]. We have proposed a qualitative mechanism based on the assumption that visible light will populate a low-lying MLCT state upon irradiation of $[Ru(phen)_2(dppz)]^{2+}$ and an IL state localized on the dppz ligand upon irradiation of $[Ru(tap)_2(dppz)]^{2+}$. In the latter case the formation of a very unstable species $[Ru(tap)_2(d^{-}ppz^{+})]^{2+}$ available for a competitive electron transfer from the guanine to the Ru(II) complex will prevent emissive processes via the low-lying triplet states as in $[Ru(phen)_2(dppz)]^{2+}$. However, according to the time-scale of the electron transfer process (~480 ps) a mechanism via the singlet states is highly improbable.

Our goal is to present a refined theoretical study that is more realistic and complete in investigating the absorption spectroscopy of both complexes in various environments (H_2O, CH_3CN, guanine–cytosine base pairs) by means of TD–DFT/PCM and QM/MM calculations. The purpose of this theoretical analysis is to explore a broad range of transition energies from 450 nm to 260 nm, never looked at in previous investigations, to compare the electronic spectra of $[Ru(phen)_2(dppz)]^{2+}$ and $[Ru(tap)_2(dppz)]^{2+}$ and to follow the trends when going from the isolated complexes in vacuum to various environments. Aside from the important aspects considered in this paper, the nature of the low-lying triplet states is also of great interest and plays an important role in the photophysics at longer time-scales and will be published elsewhere.

2. Computational details

The geometrical structures of Δ- and Λ-enantiomers $[Ru(L)_2(L')]^{2+}$ (L = phen or tap and L' = dppz) complexes were optimized in vacuum and solvent corrected models (for water and acetonitrile) for the closed shell electronic ground state at DFT (BL3LYP) level within the C_1 symmetry [27]. In order to take into account solvent effects, the Polarizable Continuum Model (IEF-PCM) with UA0 atomic radii was employed [28]. Hybrid Quantum Mechanics/Molecular Mechanics (QM/MM) [29] calculations were used to optimize the ground state structures of these complexes intercalated in both the major and minor grooves of DNA using a two-base pair model. Initial geometries for the dinucleotide sequence (5′-GC-CG-3′) have been created with the nucleic program of Tinker [30] software using the conventional geometrical parameters of B-DNA (Scheme 1). QM/MM calculations were performed with our local modified version of the Gaussian 03 package [31] linked to the Tinker software [30] for the MM calculations. Full geometry optimizations were performed. The hydrogen bonding is taken into account by means of the QM/MM method used in the present work. Whereas this reduced model is adequate to describe local properties such as optical properties it is certainly too limited and not realistic enough to discuss in detail the binding modes between DNA and the Ru(II) complexes which depend on the size of the DNA strand.

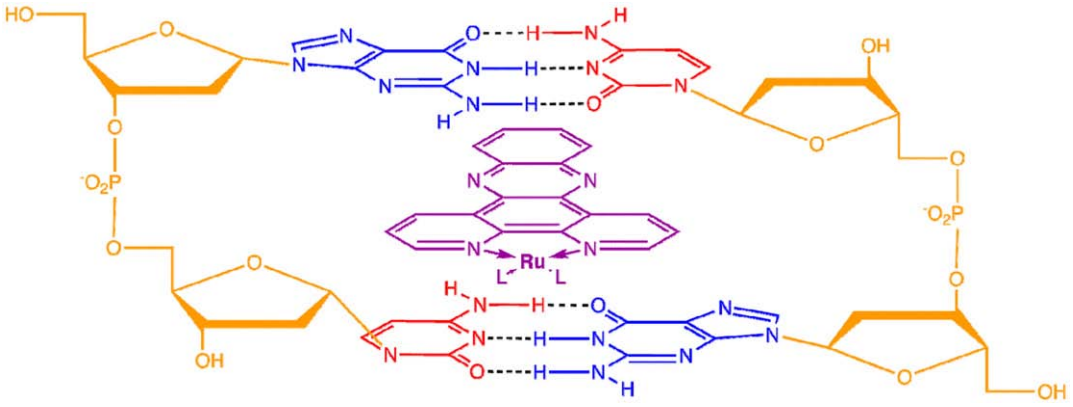

Scheme 1. Intercalated Ruthenium complex in double-stranded DNA fragment (CG–GC).

The theoretical electronic absorption spectra have been obtained by means of time-dependent DFT method (TD–DFT) applied to the optimized geometrical structures of the electronic ground state for both complexes. Even though failures of TD–DFTT in describing correctly long range transfer states in large systems [32] the absorption spectra of Ru (II) and Re(I) complexes are usually well reproduced [33,34]. For TD–DFT calculations using SCRF solvation model, the nonequilibrium PCM method was selected [35]. The solvent corrections do not take into account the specific hydrogen bonding effects.

The following basis sets and pseudopotentials describing the core electrons of the metal center were used: a polarized split valence 6-31G* basis set (10 s, 4p, 1d) contracted to [3 s, 2p, 1d] for C and N atoms and (4 s) contracted to [2 s] for H atoms [36] with Wood–Boring quasi relativistic MWB pseudopotentials and associated valence basis sets (8 s, 7p, 6d) contracted to [6 s, 5p, 3d] for the Ru atom [37]. The MM surrounding is described by the Amber99 force field for nucleic acids [38,39]. The van der Waals parameters for the QM atoms are set to the values defined for the corresponding atom type of the force field, except for the Ru atom where we have used the parameters of Ref. [40] ($R^* = 2.34$ and $\varepsilon = 0.438$).

The present model is oversimplified, based on an intercalated metal complex into a small fragment of DNA. The first step towards a more realistic model would be to increase the number of base pairs before to include water molecules into the grooves. At this stage the Ru-complexes have been treated at the QM level whereas the base pairs have been modelled by MM including electrostatic effects. Our aim is not to conclude about enantiomers relative binding energies and associated selectivity's. For this purpose at least two base pairs should be included in the QM part which is beyond our computers capabilities. However the TD–DFT results are sensitive to the electrostatic field of the MM part. This computational strategy will provide a representation featuring the influence of nearby base pairs on the structures and spectra of Ru-complexes when intercalated in the minor or major groove. This model will be transferred to the oligonucleotide sequence according to the protocol developed in the local modified version of Gaussian03 linked to Tinker and applied recently to electron-induced DNA single strand breaks [41]. In contrast to previous theoretical studies [24–26] the present work focuses on the singlet states between 450 nm and 260 nm and gives a tentative assignment of the complete experimental spectra for the two most investigated Ru(II) polypyridyl complexes in water, acetonitrile and intercalated in DNA.

3. Structure and intercalation mode of $[Ru(phen)_2(dppz)]^{2+}$ and $[Ru(tap)_2(dppz)]^{2+}$ in guanine–cytosine base pairs

The geometry of the optimized structures is based on two types of features: the local geometrical features of the Ru(II) complexes and the global features of the two-base pair model. The complexes along with the aforementioned geometries are presented in Table 1.

The Ru–N_x ($x = 1$–6; cf. Scheme 2) bond lengths have been investiged for the phen and tap complexes intercalated in DNA and are compared with those values reported in Ref. 27 for the complexes in vacuum, water, and acetonitrile. The DNA intercalated optimized tap complexes have values that range between 2.083 and 2.117 Å while similarly those for the phen complex are between 2.097 and 2.118 Å and compared well with similar complexes that have been investigated using X-ray technics $[Ru(dmp)_2(dppz)]^{2+}$ [42] with values of 2.05–2.08 Å and $[Ru(tap)_3]^{2+}$ [42] and 2.094–2.125 Å. The angles N_xRuN_y ($x = 1,3,5$; $y = 2,4,6$) for the intercalated complexes maintains the general trend that the angle between the metal center and the dppz ligand N_1RuN_2 is smaller than those for the ancillary ligands N_3RuN_4 and N_5RuN_6. The tap complex NruN angles range from 78.71 to 79.54 Å while those for the phen complex range from 78.68 to 79.05 Å which are comparable to the experimental X-ray values (tap [42]: 79.4–80.6 Å; phen [42]: 78.85–79.41 Å).

The global geometries are referenced by the distance between the centroids of the nucleobases (G = Guanine, C = Cytosine) within (e.g. G1–C1) and between (e.g. G1–C2) the base pairs. The centroids are placed in the center of the six-membered rings. The planes of the nucleobases are also formed from the same six-membered rings and are used to measure the angle of the nucleobases within each base pair. The distances between the nucleobases within a base pair for all investigated complexes range between 5.46 and 5.62 Å as compared to the Tinker DNA geometry of 5.65 Å are smaller. This decrease in distance is due to the angular change between the planes of the nucleobases that greatly vary in angles of 7.7 to 40.1° (cf. Tinker ∠PG1–PC1 = ∠PG2–PC2 = 1.3°). The change in angle is naturally due to the intercalation of the complex which consequently has the effect of doubling the distance between the two-base pairs. The Δ-complex intercalated in the major groove produce a distance between the base pairs similar to the Λ-complexes in the minor groove (6.95–7.88 Å) and vice-versa (6.62–7.23 Å).

Whereas the Δ-$[Ru(phen)_2(dppz)]^{2+}$ major, minor and Λ-$[Ru(phen)_2(dppz)]^{2+}$ minor structures are close energetically within

Table 1
Optimized local and global geometrical features of intercalated Δ- and Λ-enantiomers of $[Ru(phen)_2(dppz)]^{2+}$ and $[Ru(tap)_2(dppz)]^{2+}$ complexes in DNA are presented. The distance (Å) between centroids located in the six-membered rings of the nucleobases, e.g. G1–C1 denotes the distance between the centroids of guanine and cytosine in the first (1) base pair. The angles (°) are formed from the planes (P) and are denoted as ∠PG1–PC1. The torsion is given as the angle between the phenanthroline nitrogen atoms (N_1 and N_2) and the farthest two carbon components of the dppz ligand. The converged energy of each complex is also given (hartree) and the relative energy in (kJ mol^{-1}).

	Δ-phen maj	Δ-tap maj	Δ-phen min	Δ-tap min	Λ-phen maj	Λ-tap maj	Λ-phen min	Λ-tap min
Global								
G1–C1	5.48	5.51	5.50	5.53	5.62	5.47	5.56	5.46
G2–C2	5.49	5.50	5.50	5.61	5.54	5.61	5.56	5.48
G1–C2	7.69	7.73	6.68	6.80	6.62	6.93	7.65	7.12
G2–C1	7.88	7.73	6.68	7.23	6.84	6.67	7.01	6.95
∠PG1–PC1	32.2	28.2	35.2	31.6	7.7	36.9	26.8	40.1
∠PG2–PC2	33.0	29.2	35.9	12.3	28.1	8.1	29.1	39.0
Local								
$Ru–N_1$	2.110	2.112	2.118	2.112	2.109	2.109	2.118	2.105
$Ru–N_2$	2.113	2.111	2.118	2.108	2.112	2.117	2.097	2.101
$Ru–N_3$	2.106	2.111	2.102	2.083	2.099	2.111	2.098	2.105
$Ru–N_4$	2.104	2.104	2.103	2.109	2.106	2.105	2.103	2.112
$Ru–N_5$	2.107	2.105	2.103	2.111	2.102	2.106	2.115	2.112
$Ru–N_6$	2.110	2.114	2.102	2.109	2.110	2.098	2.108	2.095
N_1RuN_2	78.90	78.91	78.75	78.99	78.68	78.71	78.80	78.98
N_3RuN_4	79.05	79.54	78.99	79.55	78.77	78.77	78.89	79.23
N_5RuN_6	78.91	79.41	78.96	79.38	78.90	78.79	78.75	79.34
Torsion-dppz	3.7	0.7	-11.5	2.5	8.0	7.0	-1.4	-0.8
E (hartree)	−2150.13439	−2214.23634	−2150.14107	−2214.21603	−2150.11871	−2214.20606	−2150.13819	−2214.20761
Rel. energy	17.5	0.0	0.0	53.3	58.5	79.5	7.6	75.4

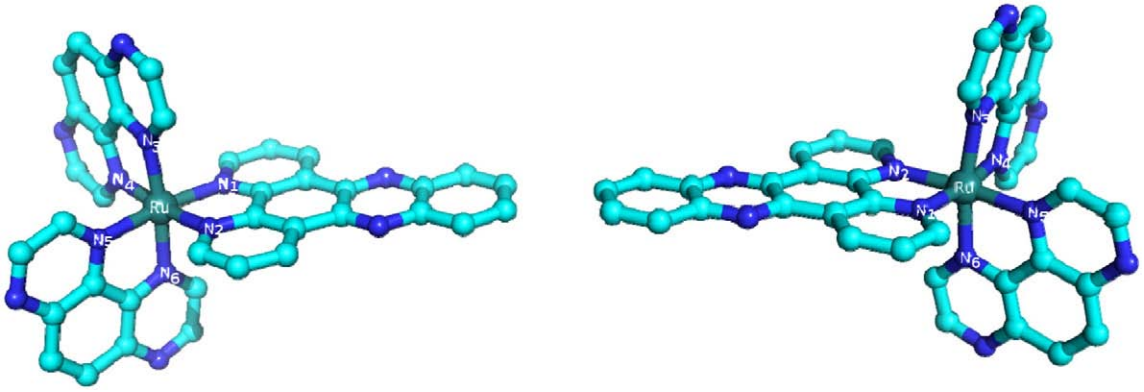

Scheme 2. Depiction of Λ- and Δ-$[Ru(tap)_2(dppz)]^{2+}$ stripped of the hydrogen atoms used as a reference to the optimized geometrical features.

18 kJ mol^{-1}, the Λ-$[Ru(phen)_2(dppz)]^{2+}$ major structure is destabilized by about 58 kJ mol^{-1} with respect to the more stable structure, namely the Δ-$[Ru(phen)_2(dppz)]^2$ complex intercalated in the minor groove (Fig. 1). The Δ-$[Ru(tap)_2(dppz)]^{2+}$ complex intercalated in the major groove (Fig. 2) is overstabilized by about 53 kJ mol^{-1} with respect to the minor groove structure. Similarly to the phen complexes the Λ enantiomers are destabilized with respect to the Δ structures with an energy gap of 75 kJ mol^{-1}. The torsion angle of the dppz appears not to have a direct effect on the energy.

In all QM/MM structures the HOMO is localized on the dppz ligand (π_{dppz}) whereas the four low-lying orbitals are localized on the ancillary ligands (π^*_{phen} and π^*_{tap}) as can be seen in Fig. 3. This is in contrast to the bonding properties in vacuum or in solvent (H_2O and CH_3CN), where in H_2O the HOMO is localized on the ancillary ligands (phen or tap) and the low-lying unoccupied orbitals are delocalized over the ancillary/dppz ligands. The later delocalization is also seen in vacuum and acetonitrile.

The π^*_{dppz} are destabilized with respect to the π^*_{phen} by intercalation. In the Δ-intercalated structures the HOMO-1, HOMO-2, HOMO-3 and HOMO-4 show a large mixed character with important delocalization on $4d_{Ru/dppz/anc}$ (anc = phen or tap). This effect is more pronounced for the phen complex. These stabilizing interactions disappear in the less stable Λ structures characterized by localized high-lying occupied orbitals.

4. Theoretical absorption spectroscopy of $[Ru(phen)_2(dppz)]^{2+}$ and $[Ru(tap)_2(dppz)]^{2+}$

4.1. Free complexes and solvent corrections

The TD–DFT electronic absorption spectra of the free complexes calculated in vacuum and with solvent corrections for water and acetonitrile are reported in Tables 2, 3 for the phen and tap substituted complexes, respectively. The position of the experimental bands is recorded for comparison. The vertical excitation energies have been calculated for the electronic ground state DFT (B3LYP) optimized structures described in ref. [27]. Only the transitions calculated with oscillator strengths greater than 0.05 are reported in the tables. A few states with very low oscillator strengths (between 0.05 and 0.01) are also indicated when necessary for the discussion.

Whereas the calculated spectra of the isolated molecules in vacuum are at odds in several respects, energetically and by the nature of the transitions, the solvent corrected spectra are more consistent. The theoretical spectra corrected for water and for acetonitrile are similar and in accordance with the experimental findings. In the case of $[Ru(tap)_2(dppz)]^{2+}$ the experimental absorption data are nearly the same in water and acetonitrile with a very small red shift of the band at about 360 nm when going from CH_3CN to H_2O. This region of the experimental spectrum is more puzzling in the case of $[Ru(phen)_2(dppz)]^{2+}$ with three bands at 368, 360 and 352 nm in CH_3CN and one band and one shoulder (denoted by sh) at 372 nm and 358 nm, respectively, in water. The upper part of the experimental spectra differs by the resolution of a band at 264 nm in the phen substituted complex, not shown in the tap complex.

In agreement with the theoretical work of [24] the band observed at 440 nm in the spectrum of $[Ru(phen)_2(dppz)]^{2+}$ is assigned to a superposition of $MLCT_{dppz}$ and $MLCT_{phen}$ excited states calculated between 454 nm (450 nm in CH_3CN) and 399 nm (398 nm in CH_3CN). The lowest singlet state calculated at about 450 nm is purely $MLCT_{dppz}$ in character. In contrast the lowest part of the spectrum of $[Ru(tap)_2(dppz)]^{2+}$ is characterized by a series of $MLCT_{tap}$ transitions calculated between 419 nm (432 nm in CH_3CN) and 404 nm (403 nm in CH_3CN) which should contribute to the band observed at 412 nm. The latter states calculated at 403 nm in water and 404 nm in acetonitrile are dominant with oscillator strengths of 0.13 and 0.12, respectively. There is no theoretical evidence of weak absorption at about 450 nm in water but two $MLCT_{tap}$ transitions are present in the acetonitrile corrected spectrum of the tap substituted complex at 452 nm and 451 nm with

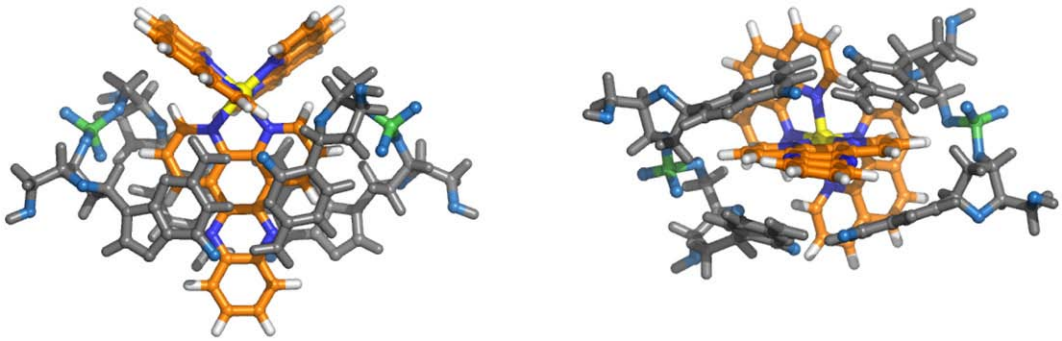

Fig. 1. Optimized geometries of Δ-$[Ru(phen)_2(dppz)]^{2+}$ minor groove (a) top view (b) side view, the most stable structure.

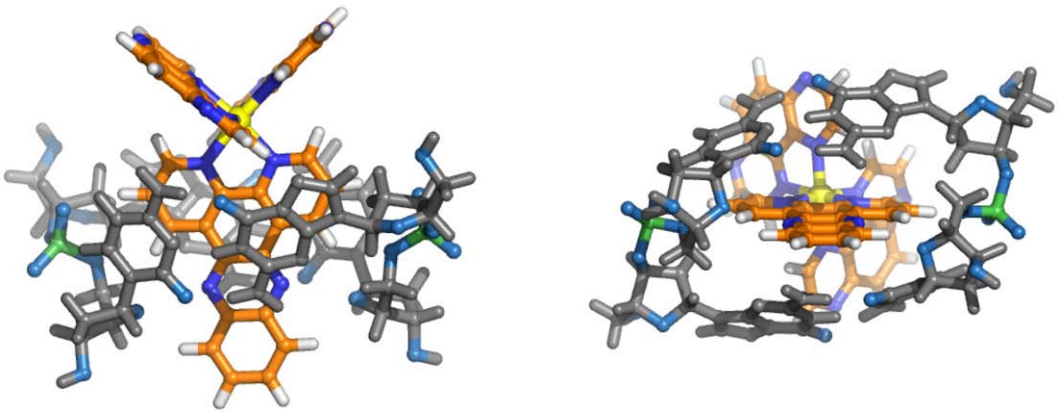

Fig. 2. Optimized geometries of Δ-$[Ru(tap)_2(dppz)]^{2+}$ major groove (a) top view (b) side view, the most stable structure.

very small oscillator strengths (10^{-4}–10^{-5}). In contrast to $[Ru(phen)_2(dppz)]^{2+}$ there is no significant contribution of the $MLCT_{dppz}$ in the lowest part of the spectrum of $[Ru(tap)_2(dppz)]^{2+}$. This is explained by the accentuated π-acceptor character of the ancillary ligands when going from the phen to the tap substituted complex.

The upper bands observed at 278 nm (276 nm in CH_3CN) and 264 nm in the spectrum of $[Ru(phen)_2(dppz)]^{2+}$ are assigned to IL states localized on the dppz and phen ligands and calculated at 280 nm (282 in CH_3CN) and 255 nm, respectively. Similarly a series of IL transitions localized either on the dppz or on the tap ligand contribute to the experimental band observed at 278 nm in the spectrum of $[Ru(tap)_2(dppz)]^{2+}$.

The assignment of the region around 360 nm, on the basis of the theoretical results reported in Tables 2 and 3, is more problematic. In the most simple case, namely $[Ru(tap)_2(dppz)]^{2+}$, a mixed $MLCT_{dppz/tap}$ transition is calculated at 390 nm in H_2O and 388 nm in CH_3CN with an oscillator strength of 0.29. This transition is followed by a series of other MLCT states localized predominantly on the dppz ligand calculated between 374 nm and 322 nm (in H_2O) and between 376 nm and 327 nm (in CH_3CN) with low oscillator strengths (<0.05). The IL_{dppz} states calculated at 382 nm and 324 nm with large oscillator strengths in vacuum were affected by the solvent corrections leading to weakly absorbing states (f<0.05) calculated at 336 nm in both solvent and at 387/376 nm in CH_3CN. These results confirm the sensitivity of this type of excited state in a solvent environment.

In $[Ru(phen)_2(dppz)]^{2+}$ $MLCT_{phen}$ and $MLCT_{dppz}$ transitions are calculated between 392 nm and 337 nm (in H_2O) and between 390 nm and 338 nm (in CH_3CN). The IL_{dppz} state is calculated at 337 nm (338 nm in CH_3CN) with oscillator strengths of 0.14 and 0.12, respectively. According to the calculated oscillator strengths the $MLCT_{phen}$ and IL_{dppz} dominate the region of the spectrum of $[Ru(phen)_2(dppz)]^{2+}$ around 360 nm. A series of LLCT and IL states largely mixed and localized either on the ancillary ligands or on the dppz ligand are found in the 300 nm–290 nm region with very large oscillator strengths for the $LLCT_{dppz}$ transitions in CH_3CN. The band observed at 316 nm in acetonitrile, reduced to a shoulder at 318 nm in water, could be attributed to this series of transitions.

The differences in the theoretical absorption spectra of $[Ru(phen)_2(dppz)]^{2+}$ and $[Ru(tap)_2(dppz)]^{2+}$ are a consequence of the localization in terms of Kohn–Sham orbitals belonging to the ancillary ligands and to the dppz ligand. Indeed in the tap substituted complex the strong π-accepting capability of the ancillary ligand leads to MLCT states with well distinguished characters, localized either on the tap ligands or on the dppz ligand. The mixing between the electronic states occurs in the upper part of the spectrum only. In contrast the spectrum of $[Ru(phen)_2(dppz)]^{2+}$ is more complicated with the presence of mixed states already in the visible energy domain. The IL_{dppz} states, sensitive to the environment, are difficult to determine. They do not seem to contribute significantly to the visible spectra of the investigated complexes. For the tap complex they were found to be of importance in vacuum but they decrease in intensity when the solvent corrections are taken into account.

One explanation could be that the crude solvent model used in the present study is reasonable for the MLCT states but inadequate for these intra-ligand states. As illustrated in the next section by the results obtained for the complexes intercalated in the guanine–cytosine base pairs the singlet IL states are stabilized by this environment and calculated at about 360 nm in agreement with the experimental findings.

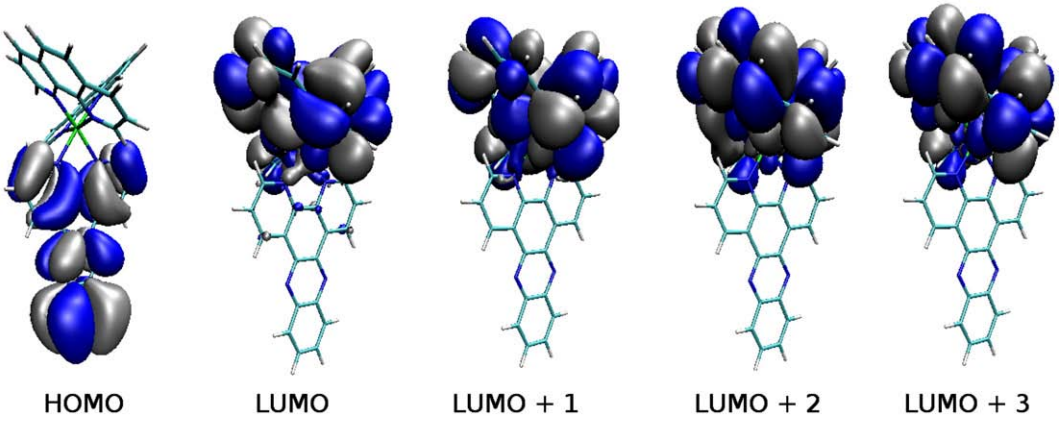

Fig. 3. Molecular orbitals for Λ-$[Ru(phen)2dppz]^{2+}$ minor groove which are representative for all complexes investigated in the present study.

Table 2
TD–DFT transition energies (in nm) to the low-lying singlet excited states of $[Ru(phen)_2(dppz)]^{2+}$ in vacuum and solvent corrected for H_2O ($\varepsilon = 78.39$) and CH_3CN ($\varepsilon = 36.64$). The calculated oscillator strengths are given in italic and the experimental bands observed in H_2O and in CH_3CN [13] are reported for comparison.

Experimental absorption data in H_2O/CH_3CN	Vacuum	H_2O	CH_3CN
440/440		$MLCT_{dppz}$ 454 *0.08*	$MLCT_{dppz}$ 450 *0.10*
	$MLCT_{phen}$ 423 *0.04*	$MLCT_{phen/dppz}$ 414 *0.08*	$MLCT_{dppz/phen}$ 413 *0.09*
	$MLCT_{dppz}$ 411 *0.17*	$MLCT_{dppz/phen}$ 409 *0.11*	$MLCT_{dppz/phen}$ 408 *0.10*
	IL_{dppz} 410 *0.01*	$MLCT_{phen}$ 399 *0.07*	$MLCT_{phen}$ 398 *0.07*
	$MLCT_{phen}$ 402 *0.04*		
	$MLCT_{phen}$ 392 *0.07*	$MLCT_{dppz}$ 392 *0.04*	$MLCT_{dppz}$ 390 *0.02*
372/368	$MLCT_{phen/dppz}$ 378 *0.05*	$MLCT_{phen}$ 387 *0.09*	$MLCT_{phen}$ 386 *0.08*
358_{sh}/360−/352		$MLCT_{dppz}$ 366 *0.04*	$MLCT_{phen}$ 386 *0.11*
	$MLCT_{dppz}/LLCT_{phen}$ 340 *0.04*	IL_{dppz} 337 *0.14*	IL_{dppz} 338 *0.12*
			IL_{dppz} 330 *0.03*
318_{sh}/316	IL_{dppz} 304 *0.88*		$LLCT_{phen}$ 300 *0.08*
		$LLCT_{phen}$ 298 *0.10*	$LLCT_{dppz}$ 295 *0.27*
		$IL_{phen}/LLCT_{dppz}$ 292 *0.09*	$IL_{phen/dppz}/LLCT_{dppz}$ 293 *0.36*
		IL_{dppz} 291 *0.17*	
		$IL_{phen}/LLCT_{dppz}$ 290 *0.05*	$LLCT_{dppz}$ 292 *0.68*
		IL_{dppz} 280 *0.03*	IL_{dppz} 282 *0.01*
$278_{sh}/276_{sh}$	$IL_{dppz}/LLCT_{dppz}$ 271 *0.10*		
264/264	$IL_{dppz}/LLCT_{dppz}$ 268 *0.08*	IL_{phen} 265 *0.06*	$IL_{phen/dppz}$ 265 *0.02*

4.2. Complexes intercalated in guanine–cytosine base pairs

Whatever the intercalation mode is, major or minor grooves, the theoretical spectra of both enantiomers, Δ-$[Ru(phen)_2(dppz)]^{2+}$ and Λ-$[Ru(phen)_2(dppz)]^{2+}$ reported in Table 4 and represented in Fig. 4, are characterized by the presence of low-lying $^1MLCT_{phen}$ transitions calculated between 459 nm and 402 nm. The corresponding excited states contribute to the experimental band observed at 440 nm. Whereas the energy domain compares rather well with the one obtained with solvent corrections (water or acetonitrile), namely 454–408 nm, the nature of the charge transfer is influenced by the presence of base pairs, with a change from $MLCT_{dppz}$ to $MLCT_{phen}$. Indeed the $^1MLCT_{dppz}$ states are destabilized by the environment and the lowest part of the spectrum is now purely MLCT to the phenanthroline ligands.

The spectrum of Δ-$[Ru(phen)_2(dppz)]^{2+}$ does not depend on the mode of intercalation and is nearly identical with a negligible difference in the calculated oscillator strengths due to altered $4d_{Ru}$/ligands mixing with accentuated delocalization on the dppz ligand in the case of the major groove mode. A significant contribution of a mixed $^1LLCT_{phen}/^1MLCT_{phen}$ state at 413 nm ($f = 0.17$) characterizes the spectrum of Λ-$[Ru(phen)_2(dppz)]^{2+}$ intercalated in the minor groove. As expected the transitions corresponding to excitations to the dppz ligands, namely the $^1MLCT_{dppz}$ and $^1IL_{dppz}$ states are very sensitive to the intercalation in the cytosine–guanine base pairs. The $^1IL_{dppz}$ states, contributing to the observed weak band at 370 nm and to the small peak at 360 nm, are stabilized and decreased in intensity as compared to the theoretical spectra in water or acetonitrile. They show some mixing with the $MLCT_{dppz}$ state in the Λ conformation. The assignment of the upper bands observed at ~300–290 nm and 266 nm on the basis of the TD–DFT results is more difficult. Interestingly the theoretical spectrum of the Δ conformer intercalated in the minor groove fits perfectly with the experimental spectrum observed in the calf thymus DNA, as illustrated in Fig. 4 (black spectrum) with four states calculated at 300 nm (MLCT; $f = 0.10$), 293 nm, (IL_{phen}; $f = 0.05$), 292 nm (IL_{dppz}; $f = 0.75$) and 288 nm ($LLCT_{phen}$; $f = 0.11$) and two states at 266 nm and 265 of IL character. The agreement is less apparent for the other structures, especially for the Λ conformer intercalated in the major groove as illustrated in Table 4 and in Fig. 4 (blue spectrum). Clearly a large mixing of MLCT, LLCT and IL states contribute to the band at 300–290 nm. In contrast to Δ-$[Ru(phen)_2(dppz)]^{2+}$, the calculated spectrum of Λ-$[Ru(phen)_2(dppz)]^{2+}$ exhibits two transitions at ~325 nm and ~320 nm which are not observed in the experimental spectra. On the whole the

Table 3
TD–DFT transition energies (in nm) to the low-lying singlet excited states of $[Ru(tap)_2(dppz)]^{2+}$ in vacuum and solvent corrected for H_2O ($\varepsilon = 78.39$) and CH_3CN ($\varepsilon = 36.64$). The calculated oscillator strengths are given in italic and the experimental bands observed in H_2O and in CH_3CN [13] are reported for comparison.

Experimental absorption data in H_2O/CH_3CN	Vacuum	H_2O	CH_3CN
$454_{sh}/452_{sh}$			$MLCT_{tap}$ 452 *~10^{-4}*
			$MLCT_{tap}$ 451 *~10^{-5}*
	IL_{dppz} 429 *0.01*		$MLCT_{tap}$ 432 *0.03*
	$MLCT_{tap}$ 427 *0.04*	$MLCT_{tap}$ 419 *0.09*	$MLCT_{tap}$ 417 *0.09*
412/412	$LLCT_{tap}/MLCT_{tap}$ 401 *0.10*	$MLCT_{tap}$ 410 *0.04*	
		$MLCT_{tap}$ 404 *0.13*	
			$MLCT_{tap}$ 403 *0.12*
		$MLCT_{dppz/tap}$ 390 *0.29*	$MLCT_{dppz/tap}$ 388 *0.29*
366/362	IL_{dppz} 382 *0.18*		IL_{dppz} 387 *0.01*
	IL_{dppz} 372 *0.06*		$IL_{dppz/tap}$ 376 *0.02*
	$MLCT_{tap}/LLCT_{tap}$ 362 *0.05*	$MLCT_{tap/dppz}$ 374 *0.03*	$MLCT_{dppz/tap}$ 370 *0.01*
	$MLCT_{dppz}/IL_{dppz}$ 324 *0.19*	IL_{dppz} 336 *0.04*	IL_{dppz} 336 *0.02*
		$MLCT_{dppz}$ 331 *0.04*	$MLCT_{dppz}$ 330 *0.03*
		$MLCT_{dppz}$ 322 *0.04*	$MLCT_{dppz}$ 327 *0.02*
	$MLCT_{dppz}$ 305 *0.08*		
	$MLCT_{dppz}/IL_{dppz}$ 304 *0.54*		
		$IL_{tap/dppz}$ 294 *0.57*	IL_{dppz} 296 *1.08*
		$IL_{dppz/tap}$ 293 *0.58*	IL_{tap} 294 *0.12*
278/278		IL_{tap} 293 *0.19*	IL_{tap} 293 *0.03*
		$IL_{dppz/tap}$ 285 *0.06*	IL_{tap} 284 *0.10*

Table 4
TD–DFT transition energies (in nm) to the low-lying singlet excited states of Δ and Λ-$[Ru(phen)_2(dppz)]^{2+}$ intercalated in guanine–cytosine base pairs. The calculated oscillator strengths *f* are given in italic and the experimental bands observed in the presence of calf thymus DNA are reported for comparison. (In bold the states with f>0.1).

Experimental absorption	Δ Major groove	Δ Minor groove	Λ Major groove	Λ Minor groove
440	$^1MLCT_{phen}$ 459 *0.02*	$^1MLCT_{phen}$ 455 *0.05*		$^1MLCT_{phen}$ 454 *0.02*
	$^1MLCT_{phen}$ 449 *0.07*	$^1MLCT_{phen}$ 446 *0.02*	$^1MLCT_{phen}$ 450 *0.05*	$^1MLCT_{\mathbf{phen}}$ **432 *0.12***
	$^1MLCT_{phen}$ 432 *0.09*	$^1MLCT_{\mathbf{phen}}$ **432 *0.12***	$^1MLCT_{phen}$ 426 *0.06*	$^1LLCT_{\mathbf{phen}}/^1MLCT_{\mathbf{phen}}$ **413 *0.17***
	$^1MLCT_{\mathbf{phen}}$ **409 *0.12***	$^1MLCT_{\mathbf{phen}}$ **407 *0.14***	$^1MLCT_{\mathbf{phen}}$ **402 *0.12***	$^1MLCT_{phen}$ 409 *0.02*
370 w	$^1IL_{dppz}$ 374 *0.02*	$^1IL_{dppz}$ 378 *0.01*	$^1MLCT_{phen}/^1LLCT_{phen}$ 381 *0.03*	
				$^1IL_{dppz}/^1MLCT_{dppz}$ 377 *0.01*
360	$^1MLCT_{dppz}$ 360 *0.07*	$^1MLCT_{dppz}$ 363 *0.08*	$^1IL_{dppz}$ 362 *0.06*	
			$^1MLCT_{dppz}$ 331 *0.02*	
			$^1IL_{dppz}/^1MLCT_{dppz}$ 324 *0.08*	$^1LLCT_{phen}/^1MLCT_{dppz}$ 326 *0.03*
				$^1IL_{dppz}/^1MLCT_{dppz}$ 319 *0.04*
	$^1MLCT_{dppz}$ 300 *0.05*	$^1MLCT_{\mathbf{dppz}}$ **300 *0.10***	$^1IL_{\mathbf{phen}}/^1LLCT_{\mathbf{phen}}/^1MLCT_{\mathbf{dppz}}$ **308 *0.23***	$^1IL_{phen}/^1MLCT_{phen}$ 295 *0.05*
~300–290	$^1MLCT_{phen}$ 299 *0.09*	$^1MLCT_{phen}$ 298 *0.03*	$^1IL_{\mathbf{phen}}$ **307 *0.14***	
		$^1IL_{phen}$ 293 *0.05*	$^1IL_{\mathbf{phen}}/^1MLCT_{\mathbf{dppz}}$ **307 *0.24***	$^1IL_{\mathbf{dppz}}/^1MLCT_{\mathbf{dppz}}$ **289 *0.58***
	$^1LLCT_{\mathbf{phen}}$ **294 *0.37***	$^1IL_{\mathbf{dppz}}$ **292 *0.75***		
	$^1LLCT_{\mathbf{phen}}$ **291 *0.42***	$^1LLCT_{\mathbf{phen}}$ **288 *0.1***		$^1MLCT_{\mathbf{dppz}}/^1MLCT_{\mathbf{phen}}/^1IL_{\mathbf{dppz}}$ **289 *0.34***
		$^1IL_{dppz}$ 266 *0.05*		$^1IL_{\mathbf{dppz}}$ **265 *0.14***
266		$^1IL_{\mathbf{phen}}$ **265 *0.20***		$^1LLCT_{dppz}$ 261 *0.07*

theoretical spectra of Λ-$[Ru(phen)_2(dppz)]^{2+}$ and Δ-$[Ru(phen)_2(dppz)]^{2+}$ differ significantly in contrast to the experimental findings [4], the latter being in better accord with the observed spectra. The good agreement between the theoretical and experimental spectra obtained for Δ-$[Ru(phen)_2(dppz)]^{2+}$ intercalated either in the minor or in the major groove is illustrated in Fig. 4, where the experimental bands are represented by black sticks.

The main difference between the theoretical spectra calculated in water and in the cytosine–guanine bases pair is the nature of the lowest states absorbing in the visible domain of energy. These states correspond to a charge transfer to the dppz ligand in water and to the phen ancillary ligands when intercalated. This is certainly one explanation to the low quantum yield of luminescence in water which becomes moderate in acetonitrile and increases with intercalation in DNA. Indeed, absorption in water will populate the $MLCT_{dppz}$ state leading to a transfer of electronic density on the dppz ligand with the formation of a formal $dppz^{\bullet}$ localized species with phenazine azanitrogens easily accessible to hydrogen bonding. In contrast and despite the similarity of the theoretical absorption spectra in water and in acetonitrile (Table 2) a total quenching of luminescence cannot occur without hydrogen bonding solvents such as acetonitrile. When the complex is intercalated the absorption is more likely to occur through the $MLCT_{phen}$ states, according to the results reported in Table 4. The population of this charge transfer excited state towards the ancillary ligands is not electronically favourable to the formation of hydrogen bonding between water and the non-coordinating phenazine nitrogens of the dppz ligand. This confirms the early experimental explanation to the undetectable emission of $[Ru(phen)_2(dppz)]^{2+}$ in water enhanced when intercalated in DNA [20].

According to the results obtained for $[Ru(tap)_2(dppz)]^{2+}$ in water, acetonitrile and intercalated in guanine–cytosine base pairs (Tables 3, 5) the possibility of hydrogen bonding to the non-coordinating phenazine nitrogens of the dppz ligands after absorption in the visible is unlikely since the lowest MLCT excited states correspond to charge transfer to the tap ancillary ligands whatever the environment is. Indeed this compound is luminescent in water as well as in acetonitrile. The quenching of luminescence observed for the tap complex when intercalated in DNA is more likely due to different properties of the low-lying triplet excited states as proposed on the basis of experimental

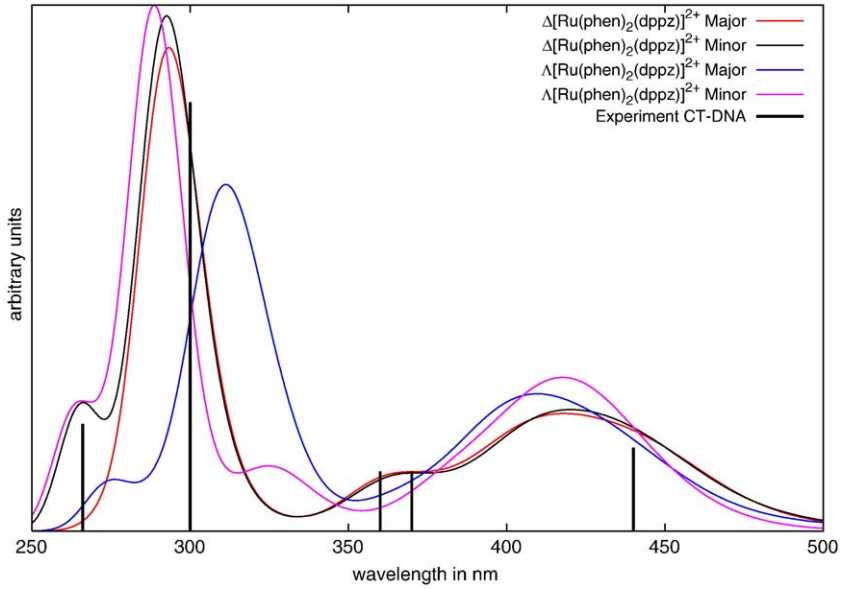

Fig. 4. Theoretical TD-DFT absorption spectra of Δ and Λ-$[Ru(phen)_2(dppz)]^{2+}$ intercalated in guanine–cytosine base pairs together with experimental bands (in black). The spectra have been artificially broadened using 2000 cm^{-1} (FWHM) wide Gaussian lineshapes.

Table 5
TD–DFT transition energies (in nm) to the low-lying singlet excited states of Δ and Λ-$[Ru(tap)_2(dppz)]^{2+}$ intercalated in guanine–cytosine base pairs. The calculated oscillator strengths are given in italic and the experimental bands observed in the presence of calf thymus DNA are reported for comparison. (in bold the states with f>0.1)

Experimental absorption	Δ Major groove		Δ Minor groove		Λ Major groove		Λ Minor groove	
462	$^1MLCT_{tap}$	466 *0.03*						
			$^1MLCT_{tap}$	453 *0.01*	$^1LLCT_{tap}$	446 *0.02*	$^1LLCT_{tap}$	454 *0.05*
	$^1MLCT_{tap}$	443 *0.06*	$^1MLCT_{tap}$	441 *0.03*	$^1MLCT_{tap}$	445 *0.07*		
							$^1MLCT_{tap}$	430 *0.01*
420	$^1MLCT_{\mathbf{tap}}$	**422 *0.10***	$^1MLCT_{\mathbf{tap}}$	**421 *0.11***	$^1MLCT_{tap}$	424 *0.03*	$^1MLCT_{tap}$	423 *0.04*
			$^1MLCT_{tap}/^1LLCT_{tap}$	412 *0.03*	$MLCT_{tap}$	409 *0.08*	$^1MLCT_{tap}/^1LLCT_{tap}$	400 *0.06*
	$^1MLCT_{tap}/^1LLCT_{tap}$	392 *0.06*	$^1LLCT_{tap}/^1IL_{dppz}$	387 *0.05*	$^1IL_{\mathbf{dppz}}/^1MLCT_{\mathbf{tap}}$	**381 *0.15***	$^1MLCT_{\mathbf{tap}}/^1LLCT_{\mathbf{tap}}$	**380 *0.17***
	$^1LLCT_{tap}/^1MLCT_{tap}$	383 *0.07*						
	$^1LLCT_{tap}/$							
	$^1MLCT_{tap}$	373 *0.07*	$^1LLCT_{\mathbf{tap}}$	**376 *0.13***	$^1LLCT_{tap}$	369 *0.08*	$^1IL_{dppz}$	357 *0.01*
362	$^1IL_{dppz}$	354 *0.02*						
	$^1IL_{dppz}$	339 *0.03*	$^1IL_{dppz}$	343 *0.03*				
					$^1MLCT_{dppz}/^1IL_{dppz}$	322 *0.06*	$^1MLCT_{dppz}/^1IL_{dppz}$	318 *0.05*
	$^1MLCT_{\mathbf{dppz}}/^1IL_{\mathbf{dppz}}$	**309 *0.17***	$^1MLCT_{\mathbf{dppz}}/^1IL_{\mathbf{dppz}}$	**312 *0.20***	$^1IL_{\mathbf{dppz}}$	**316 *0.25***	$^1MLCT_{\mathbf{dppz}}/^1IL_{\mathbf{dppz}}$	**310 0.11**
					$^1IL_{tap}$	311 *0.06*		
~300	$^1LLCT_{\mathbf{tap}}$	**300 *0.53***	$^1LLCT_{\mathbf{tap}}$	**304 *0.42***	$^1LLCT_{\mathbf{tap}}$	**308 *0.26***		
	$^1IL_{dppz}/$		$^1IL_{ddpz}/$		$^1IL_{dppz}/$		$^1LLCT_{\mathbf{tap}}/^1IL_{\mathbf{dppz}}$	**300 *0.26***
	$^1MLCT_{dppz}$	290 *0.06*	$^1MLCT_{dppz}$	291 *0.08*	$^1MLCT_{dppz}$	292 0.05	$^1MLCT_{\mathbf{dppz}}/^1IL_{\mathbf{dppz}}$	**294 *0.40***

investigation [7] and confirmed by our recent theoretical calculations to be published.

The two lowest bands observed in the spectrum of $[Ru(tap)_2(dppz)]^{2+}$ are shifted to the red at 460 nm and 420 nm as compared to $[Ru(phen)_2(dppz)]^{2+}$ characterized by two bands at 440 nm and 370 nm. The theoretical spectrum of Δ-$[Ru(tap)_2(dppz)]^{2+}$ intercalated in the major groove is the only one following this trends with calculated $MLCT_{tap}$ transitions at 466 nm and 440 nm. The TD–DFT spectra of the other conformations are also characterized by low-lying $MLCT_{tap}$ excited states between 450 and 440 nm which should contribute to the band observed around 462 nm. The experimental band at 420 nm is attributed to the series of $^1MLCT_{tap}$ excited states calculated at 422 nm (Δ-enantiomer in the major groove), 421 nm (Δ-enantiomer in the minor groove), 424 nm (Λ-enantiomer in the major groove) and 423 nm (Λ-enantiomer in the minor groove). A series of mixed $^1LLCT_{tap}/^1MLCT_{tap}$ calculated between 392 nm and 412 nm could also contribute to the band at 420 nm. Similarly to $[Ru(phen)_2(dppz)]^{2+}$ the IL_{dppz} transitions contribute mainly to the absorption at 362 nm with some input of the $MLCT_{tap}$ and $LLCT_{tap}$ states. The upper part of the theoretical spectra of Δ-$[Ru(tap)_2(dppz)]^{2+}$ and Λ-$[Ru(tap)_2(dppz)]^{2+}$, at about 300 nm and beyond, is built from a superposition of MLCT/LLCT/IL states, localized either on tap or on dppz, the contribution of each depending on the conformation. As expected the $^1IL_{dppz}$ transitions in $[Ru(tap)_2(dppz)]^{2+}$ are shifted to the blue at about 350 nm with respect to $[Ru(phen)_2(dppz)]^{2+}$ characterized by low-lying ^1IL states at about 375 nm. As illustrated in Fig. 5 the four theoretical spectra obtained for $[Ru(tap)_2(dppz)]^{2+}$ do not differ significantly and the agreement with the experimental date is reasonable.

5. Conclusion

This theoretical study of the excited states properties of $[Ru(phen)_2(dppz)]^{2+}$ and $[Ru(tap)_2(dppz)]^{2+}$ in water, acetonitrile and

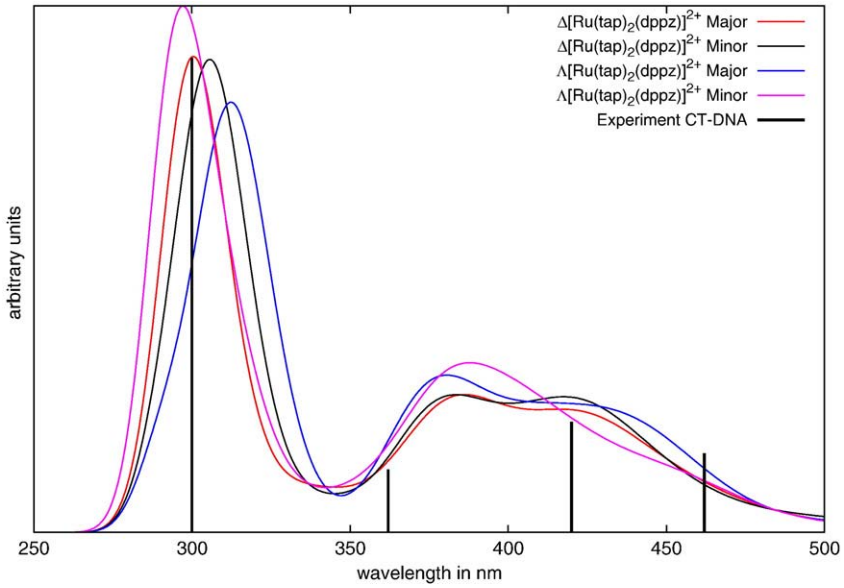

Fig. 5. Theoretical TD–DFT absorption spectra of Δ and Λ-$[Ru(tap)_2(dppz)]^{2+}$ intercalated in guanine–cytosine base pairs. The spectra have been artificially broadened using 2000 cm^{-1} (FWHM) wide Gaussian lineshapes.

intercalated in two cytosine–guanine base pairs represent the most complete exploration of the electronic absorption spectroscopy of the most studies DNA intercalators. Despite the limitation of our models and of the TD–DFT method, the only one adapted to such a complicated investigation, some general features can be extracted in a tentative rationalization of the huge amount of available experimental data.

The intercalated Δ-structures either in minor or major groove appear to be the most stable with respect to the Λ-structures within the limit of our computational model. This is due to a bending of the dppz ligand observed only in the Λ intercalated complexes. This deformation reduces the stabilizing 4dRu/dppz/anc (anc = phen or tap) interaction. The bonding and spectroscopic properties calculated in vacuum are not realistic whereas the spectra calculated with solvent corrections compare rather well with the experimental data in H_2O or CH_3CN.

Whereas the visible absorption of $[Ru(tap)_2(dppz)]^{2+}$ is governed by the $MLCT_{tap}$ transitions whatever the environment is (water, acetonitrile or bases pair), the visible absorption of $[Ru(phen)_2(dppz)]^{2+}$ is characterized by transitions to $MLCT_{dppz}$ in water and acetonitrile and to $MLCT_{phen}$ when intercalated in base pairs. This is an effect of the accentuated π-acceptor character of the tap ligand with respect to the phen ligand. Consequently the transitions involving excitations to the dppz ligand are destabilized in the tap substituted complex and the lowest part of the spectrum of $[Ru(tap)_2(dppz)]^{2+}$, as well as its luminescence properties are less sensitive to the environment.

The main features of the experimental spectra reported in DNA or synthetic polynucleotides are better reproduced by the theoretical absorption spectra of the Δ enantiomers whatever the mode of intercalation is (major or minor groove). This is especially true for $[Ru(phen)_2(dppz)]^{2+}$.

As expected the response of the IL_{dppz} state to the environment is very sensitive. In vacuum, water and acetonitrile these transitions are characterized by significant oscillator strengths and their positions depend significantly on the medium with blue shifts of about 80 nm when going from vacuum to water or acetonitrile. When the complex is intercalated in the guanine–cytosine base pairs the $^1IL_{dppz}$ contributes mainly to the band at 370 nm observed in the spectrum of $[Ru(phen)_2(dppz)]^{2+}$ and to the band at 362 nm observed in the spectrum of $[Ru(tap)_2(dppz)]^{2+}$. This excited state should not participate in the absorption to the visible energy domain and excludes the mechanism proposed in our previous work [27], namely the direct population of this state in the tap substituted complex is followed by electron transfer towards the guanine. Consequently the quenching of the luminescence of $[Ru(tap)_2(dppz)]^{2+}$ by electron transfer to the guanine should be based on the photophysics of the low-lying triplet excited states investigated in detail in one of our recent studies to be published.

Our model limited to the inclusion of two base pairs certainly underestimates the effects of the biological environment on the spectroscopic properties of the titled complexes. However, the Franck–Condon absorption is an ultra-fast process excluding significant structural relaxation effects in the excited states.

Acknowledgement

The authors are grateful to Prof A. Kirsch-De Mesmaeker and Dr C. Moucheron for helpful discussions. D. Ambrosek thanks Université Louis Pasteur and P. F. Loos the ANU Research School of Chemistry for postdoctoral fellowships. This work is part of the projects supported by the International Center for Frontier Research in Chemistry (FRC, Strasbourg) and by the PhotoBioMet ANR-09-BLAN-0191-01 funding. The calculations have been performed at the IDRIS computer center (Paris) and on the cluster of the LCQS.

References

[1] E. Frideman, J.-C. Chambon, J.-P. Sauvage, N.J. Turro, J.K. Barton, J. Am. Chem. Soc. 112 (1990) 4960–4962.
[2] R.M. Hartshorn, J.K. Barton, J. Am. Chem. Soc. 114 (1992) 5919–5925.
[3] Y. Jenkins, A.E. Friedman, N.J. Turro, J.K. Barton, Biochemistry 31 (1992) 10809–10816 and references therein.
[4] C. Hiort, P. Lincoln, B. Nordén, J. Am. Chem. Soc. 115 (1993) 3448–3454.
[5] I. Haq, P. Lincoln, D. Suh, B. Nordén, B.Z. Chowdhry, J.B. Chaires, J. Am. Chem. Soc. 117 (1995) 4788–4796.
[6] P. Lincoln, A. Broo, B. Nordén, J. Am. Chem. Soc. 118 (1996) 2644–2653.
[7] E.J.C. Olson, D. Hu, A. Hörmann, A.M. Jonkman, M.R. Arkin, E.D.A. Stemp, J.K. Barton, P.F. Barbara, J. Am. Chem. Soc. 119 (1997) 11458–11467.
[8] C. Moucheron, A. Kirsch-DeMesmaeker, J. Phys. Org. Chem. 11 (1998) 577–583.
[9] I. Ortmans, S. Content, N. Boutonnet, A. Kirsch-DeMesmaeker, W. Bannwarth, J.-P. Constant, E. Defrancq, J. Lhomme, Chem. Eur. J. 5 (1999) 2712–2721.
[10] J.M. Kelly, C.M. Creely, M.M. Feeney, S. Hudson, W.J. Blau, B. Elias, M. Towrie, A.W. Parker, Central Laser Facilities Annual Report, 2001/2002, pp. 111–114.
[11] C.G. Coates, P. Callaghan, J.J. McGarvey, J.M. Kelly, L. Jacquet, A. Kirsch-DeMesmaeker, J. Mol. Struct. 598 (2001) 15–25.
[12] B. Hwa Yun, J.-O. Kim, B. Wooklee, P. Lincoln, B. Nordén, J.-M. Kim, S.K. Kim, J. Phys. Chem. B 107 (2003) 9858–9864.
[13] I. Ortmans, B. Elias, J.M. Kelly, C. Moucheron, A. Kirsch-DeMesmaeker, Dalton Trans. (2004) 668–676.
[14] J. Olofsson, B. Önfelt, P. Lincoln, J. Phys. Chem. A 108 (2004) 4391–4398.
[15] M.K. Brennaman, T.J. Meyer, J.M. Papanikolas, J. Phys. Chem. A 108 (2004) 9938–9944.
[16] J.M. Kim, J.-M. Lee, J.Y. Choi, H. Mee Lee, S.K. Kim, J. Inorg. Biochem. 101 (2007) 1386–1393.
[17] B. Elias, C. Creely, G.W. Doorley, M.M. Feeney, C. Moucheron, A. Kirsch-DeMesmaeker, J. Dyer, D.C. Gills, M.W. Georges, P. Matousek, A.W. Parker, M. Towarie, J.M. Kelly, Chem A Eur. J. 14 (2008) 369–375.
[18] S. LeGac, S. Rickling, P. Gerbaux, E. Defrancq, C. Moucheron, A. Kirsch-DEMesmaeker, Angew. Chem. Int. Ed. 47 (2008) 1–5.
[19] L. Herman, S. Ghosh, E. Defrancq, A. Kirsch-DeMesmaeker, J. Phys. Org. Chem. 21 (2008) 670–681.
[20] C.G. Coates, J.J. McGarvey, P.L. Callaghan, M. Coletti, J.C. Hamilton, J. Phys. Chem. B 105 (2001) 730–735.
[21] D. Han, H. Wang, N. Ren, J. Mol. Struct. (TheomChem) 711 (2004) 185–192.
[22] A. Broo, P. Lincoln, Inorg. Chem. 36 (1997) 2544–2553.
[23] G. Pourtois, D. Beljonne, C. Moucheron, S. Schummm, A. Kirsch-DeMesmaeker, R. Lazzaroni, J.-L. Bredas, J. Am. Chem. Soc. 126 (2004) 683–692.
[24] S. Fantacci, F. De Angelis, A. Sgamellotti, N. Re, Chem. Phys. Lett. 396 (2004) 43–48.
[25] S. Fantacci, F. De Angelis, A. Sgamellotti, A. Marrone, N. Re, J. Am. Chem. Soc. 127 (2005) 14144–14145.
[26] E.R. Batista, R.L. Martin, J. Phys. Chem. A 109 (2005) 3128–3133.
[27] A. Atsumi, L. González, C. Daniel, J. Photochem. Photobiol. A: Chem. 190 (2007) 310–320.
[28] J. Tomasi, B. Mennucci, R. Cammi, Chem. Rev. 105 (2005) 2999–3094.
[29] A. Warshell, M. Levitt, J. Mol. Biol. 103 (1976) 227–249;
U.C. Singh, P.A. Kollman, J. Comput. Chem. 7 (1986) 718–730;
M.J. Field, P.A. Bash, M. Karplus, J. Comput. Chem. 11 (1990) 700–733.
[30] J.W. Ponder, Tinker, version 4.2, Washington University, St Louis, MO, 2004.
[31] Gaussian 03, Revision C.02, Gaussian Inc., Wallingford, CT, 2004; C. Lee, W. Yang, R. G. Parr, Phys.Rev. B37 (1988) 785–789.
[32] A. Dreuw, M. Head-Gordon, J. Am. Chem. Soc. 126 (2004) 4007–4016.
[33] J. Bossert, C. Daniel, Coord. Chem. Rev. 252 (2008) 2493–2503.
[34] J. Bossert, C. Daniel, Chem. A Eur. J. 12 (2006) 4835–4843.
[35] M. Cossi, V. Barone, J. Chem. Phys. 115 (2001) 4708–4717.
[36] P.C. Hariharan, J.-A. Pople, Theor. Chim. Acta 28 (1973) 213–222;
M.M. Franci, W.J. Pietro, W.J. Hehre, J.S. Binkley, M.S. Gordon, D.J. Defrees, J.A. Pople, J. Chem. Phys. 77 (1982) 3654–3658.
[37] D. Andrae, U. Haussermann, M. Dolg, H. Preuss, Theor. Chim. Acta 77 (1990) 123–141.
[38] W.D. Cornell, P. Cieplak, C.I. Bayly, I.R. Gould, K.M. Merz Jr., D.M. Ferguson, D.C. Spellmeyer, T. Fox, J.W. Caldwell, P.A. Kollman, J. Am. Chem. Soc. 117 (1995) 5179–5197.
[39] J. Wang, P. Cieplak, P.A. Kollman, J. Comput. Chem. 21 (2000) 1049–1074.
[40] N.L. Allinger, X. Zhou, J. Bergsma, J. Mol. Struct.- TheoChem 312 (1994) 69–83.
[41] P.F. Loos, E. Dumont, A.D. Laurent, X. Assfeld, Chem. Phys. Lett. 475 (2009) 120–123.
[42] J.G. Liu, Q.L. Zhang, X.F. Shi, L.N. Ji, Inorg. Chem. 40 (2001) 5045–5050.